Dependence of curvature type of thermal lensing on number of bounces in a zigzag slab laser: numerical modeling*

Fu Xing(付 星)†, Liu Qiang(柳 强), Yan Xing-Peng(闫兴鹏), and Gong Ma-Li(巩马理)

State Key Laboratory of Tribology, Center for Photonics and Electronics, Department of Precision Instruments, Tsinghua University, Beijing 100084, *China*

(Received 3 March 2011; revised manuscript received 20 April 2011)

The curvature type of the thermal lens generated in a zigzag slab laser is numerically analysed. It is found that the curvature type of the thermal lens varies alternatively between the convex and the concave lenses with the number of bounces of light within the slab, which can be well explained by the trace of the zigzag propagation. In addition, we conclude that the beamlet with a larger number of bounces experiences weaker thermal lensing but more serious wavefront deformation due to the large side lobe portion in the curve of optical path difference.

Keywords: thermal lensing, zigzag slab laser, curvature type

PACS: 42.55.Xi, 42.60.Jf **DOI:** 10.1088/1674-1056/20/11/114210

1. Introduction

The zigzag slab laser has attracted much attention and it has been widely researched due to its outstanding performance in power scalability and the nearly one-dimensional thermal gradient.[1−4] A 19 kW ultrahigh laser output was achieved in a coherent combination of two amplifier chains, where several end-pumped Nd:YAG zigzag slab amplifiers were used for the main stage.[5] Yasuhara *et al.*[6] reported a thermally controlled Nd:glass zigzag slab laser with a stimulated Brillouin scattering mirror, which reached an average power of 213 W at 10 Hz, corresponding to a peak power of 2.4 GW. Sridharan *et al.*[7] developed a 100 W class of Nd:YAG master oscillator power amplifier (MOPA) laser system based in part on an end-pumped zigzag slab power amplifier, besides, an economic batch fabrication technique was described. Our group[8] produced a single-pulse energy of 1.02 mJ with a high-repetition-rate and a high-pulse-energy MOPA laser system based on a two-stage Nd:YAG zigzag slab main amplifier. Also, a high power zigzag slab laser oscillator was realized by employing two Nd:YAG/YAG composite slabs in the cavity, achieving a 402 W continue wave (CW) output with an optical–optical efficiency of 35.4%.[9]

The zigzag path of the beamlet through the slab along the direction of heat removal efficiently reduces the thermally induced optical path difference (OPD), which however still exists. Several reports have dealt with the thermal lensing effect in zigzag slab lasers. Shoup *et al.*[10] estimated the thermal profile of the Brewster's angle zigzag Nd:glass slab amplifier, the stress distribution, and the thermally induced wavefront error by using the finite-element program ANSYS. Chen *et al.*[11] performed a realistic calculation of the induced lensing due to the thermal and the stress gradients in the edge-pumped Yb:YAG slab lasers for the zigzag propagation. Chung and Bass[12] carried out a thorough and general geometrical optics analysis of the slab-shaped laser gain medium with the light propagating in a zigzag manner. They also described the OPD introduced by the surface distortions across the whole aperture. In the present paper, we concentrate on the curvature type of the thermal lens formed within the zigzag slab laser based on a numerical modeling and demonstrate its dependence on the number of bounces of light, which, to the best of our knowledge, is disclosed for the first time. We first introduce the modeling of the zigzag propagation, and then calculate the temperature distribution and the OPD profile, thereby exploring the origin of the curvature-type dependence.

*Project supported by the National Natural Science Foundation of China (Grant Nos. 50721004 and 60978032).

†Corresponding author. E-mail: fu-x06@mails.tsinghua.edu.cn

© 2011 Chinese Physical Society and IOP Publishing Ltd

2. Modeling of zigzag propagation

The coordinate system and the parameters used in analysing the zigzag beam propagation within a slab laser are presented in Fig. 1, where α is the apex angle, γ is the angle between the zigzag path and the total-internal-reflection (TIR) surface, θ and β are the incident and the refractive angles respectively at the slab end, t is the thickness of the slab, L is the length of the TIR surface, and the overall slab length is $L + D_{\rm e}$. We can obtain the following equation according to the geometrical relation:

$$\gamma = \alpha - \arcsin\left(\frac{n_{\rm a}\sin\theta}{n_{\rm s}}\right), \tag{1}$$

where $n_{\rm a}$ and $n_{\rm s}$ are the refractive indices of the air and the slab, respectively. The distance along the z axis between adjacent bounces of light is indicated by $D_{\rm f} = tctg\gamma$, and the projection length at the TIR surface of the full-aperture beam is thus $D = D_{\rm e} + D_{\rm f} = t(ctg\gamma + ctg\alpha)$. The circle-marked and the square-marked arrow lines represent two edges of the full-aperture beam entering the slab. The total number of bounces N must be an even integer to avoid the aperture clipping of the beam traveling through the slab, and we can have[13]

$$L = Ntctg\gamma. \tag{2}$$

The case $N = 6$ is presented in Fig. 1. From Eqs. (1) and (2), the number of bounces for a fixed slab can be obtained for selected appropriate incident angles at the slab ends. For a better view and a more clear tracking of the laser beam within the slab, the zigzag path of light is straightened by unfolding the slab (shown by solid line) relative to the TIR surfaces into a series of mirrored images (shown by dotted line), as illustrated by Fig. 1.

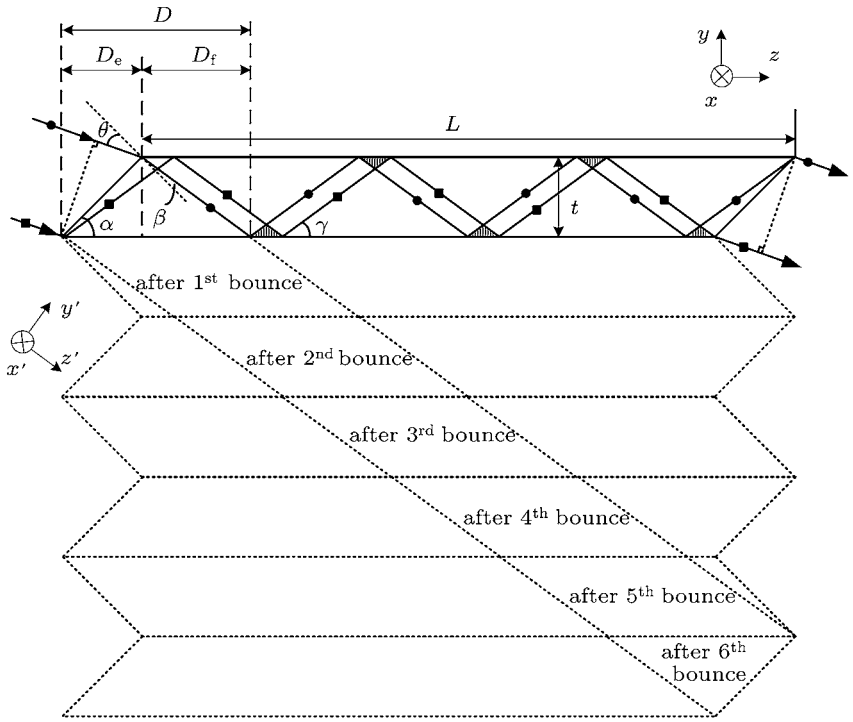


Fig. 1. Parameters and coordinate systems used in the analysis.

To investigate the thermal lensing in the slab, the optical path difference must be calculated, which can be expressed as[17]

$$D_{\rm op} = D_{\rm op,t} + D_{\rm op,e} + D_{\rm op,s}, \tag{3}$$

where $D_{\rm op,t}$ and $D_{\rm op,e}$ are caused by the thermal gradients and the end effect, respectively, and $D_{\rm op,s}$ is the OPD due to the stress-induced variation of refraction. Generally, the third term on the right-hand side of Eq. (3) is much smaller than the first and the second terms,[11,14] thus it is not included in our modeling. For the second term, the end-face deformation

is caused by the strain in a small region near the end face,[17] which can be derived from the thermal expansion theory,[15,17]

$$D_{\mathrm{op,e}}(x,y)=\mu_{\mathrm{a}}\int_0^{l_{\mathrm{e}}}[T(x,y,z)-T_0]\,\mathrm{d}z, \qquad (4)$$

where μ_{a} is the thermal expansion coefficient, $T(x,y,z)$ is the temperature distribution, T_0 is the average temperature, and l_{e} is the length of the area, in which the end-effect deformation occurs. The l_{e} is difficult to determine. Thus, $D_{\mathrm{op,e}}$ is usually calculated by defining a ratio M_{r} of $D_{\mathrm{op,e}}$ to the total OPD,[14,16,17] leading to the expression of the total OPD as

$$D_{\mathrm{op}}=\frac{D_{\mathrm{op,t}}}{1-M_{\mathrm{r}}}. \qquad (5)$$

In this paper, we take a further step to neglect $D_{\mathrm{op,e}}$ and assume $D_{\mathrm{op}}=D_{\mathrm{op,t}}$ because of two reasons. First, the Nd:YAG/YAG composite crystal under consideration has long end caps, which restrict heat generation to the central section, thus dramatically reducing the end effect.[11,18] Second, in this paper our main interest is in the dependence of curvature type of thermal lensing, which is not affected at all by the exclusion of the optical path difference due to the end effect, since the total OPD is proportional to $D_{\mathrm{op,t}}$ according to Eq. (5). Therefore, the calculation of OPD in our model is simplified into the calculation of $D_{\mathrm{op,t}}$, which can be described in the $x'y'z'$ coordinate system and is given by[17]

$$D_{\mathrm{op}}(x',y')=\frac{\mathrm{d}n}{\mathrm{d}T}\int[T(x',y',z')_{x'y'z'}-T_0]\,\mathrm{d}z, \qquad (6)$$

where $T(x',y',z')$ is the temperature distribution in the $x'y'z'$ coordinate system. Obviously, the OPD is more convenient to calculate with $T(x',y',z')$ expressed in the xyz coordinate system using the interpolation method. The transformation formula between the two systems can be derived as

$$T(x',y',z')_{x'y'z'}=T(x',\Omega,y'\sin\gamma+z'\cos\gamma)_{xyz}, \qquad (7)$$

where Ω is dependent on the number of bounces N. The Ω is given as

$$\Omega=\left|2t\left[\mathrm{ceil}\left(\frac{|z'\sin\gamma-y'\cos\gamma|}{2t}\right)\right]-(z'\sin\gamma-y'\cos\gamma)\right|, \qquad (8)$$

where $\mathrm{ceil}(m)$ returns the smallest integer not less than m. Furthermore, the focal length F_{t} of the corresponding thermal lens can be written as[11]

$$F_{\mathrm{t}}=\frac{(y-y_0)^2}{2[D_{\mathrm{op}}(y)-D_{\mathrm{op}}(y_0)]}, \qquad (9)$$

where y_0 represents the coordinate of the thickness centre.

3. Temperature distribution

In the following, the calculation of the temperature distribution within the slab is briefly described. The same crystal parameters as those of the Nd:YAG/YAG composite slab employed in the previous experiments[8,9,13] are used. The slab is measured to be 8 mm in width (w), 2 mm in thickness (t), and 76.8 mm in length (L), into which a 0.5 at.% doped 50 mm-long Nd:YAG crystal is diffused and bonded between two undoped 14.4 mm-long YAG end caps with the ends cut at $\alpha=45°$. The slab is pumped at each end by a diode stack with an output power of 1 kW, and the pumping densities in the width and the thickness directions of the cross sections are assumed to be uniform in this paper.

The three-dimensional thermal computation is performed with the software program FEMLAB based on the finite element method to solve the heat conduction equation[16]

$$k\boldsymbol{\nabla}^2T(x,y,z)+Q(x,y,z)=0, \qquad (10)$$

with boundary conditions

$$\frac{\partial T}{\partial x}=\frac{h_{\mathrm{a}}}{k}(T_{\mathrm{a}}-T)\quad\text{at } x=\pm\frac{w}{2}, \qquad (11)$$

$$\frac{\partial T}{\partial y}=\frac{h_{\mathrm{c}}}{k}(T_{\mathrm{c}}-T)\quad\text{at } y=\pm\frac{t}{2}, \qquad (12)$$

$$\frac{\partial T}{\partial z}=\frac{h_{\mathrm{a}}}{k}(T_{\mathrm{a}}-T)\quad\text{at slab ends}, \qquad (13)$$

where k is the thermal conductivity (14 $\mathrm{W\cdot m^{-1}\cdot K^{-1}}$ for Nd:YAG), $T_{\mathrm{a}}=25$ °C is the room temperature $T_{\mathrm{c}}=15$ °C is the coolant temperature, $h_{\mathrm{a}}=0$ is the free convection heat transfer coefficient at the ends and the edge faces under the assumption of heat insulation, $h_{\mathrm{c}}=10^6$ $\mathrm{W\cdot m^{-2}\cdot K^{-1}}$ is the forced convection heat transfer coefficient in the cooling faces, and Q is the heat power deposited per unit volume, which is expressed as a fraction of the absorbed pump power deposited as heat (30% for Nd:YAG).

Figure 2 shows the temperature profile in the width centre of the cross section, indicating a maximum temperature of 126.2 °C. The temperature along the slab width is quite uniform, thus the discussion of

the thermal lensing is focused on the case along the thickness direction.

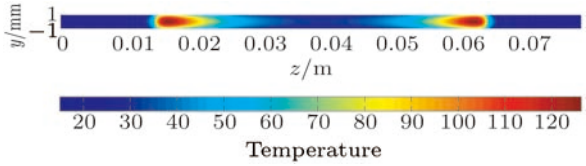


Fig. 2. (colour online) Temperature profiles in the slab cross section at $w = 0$.

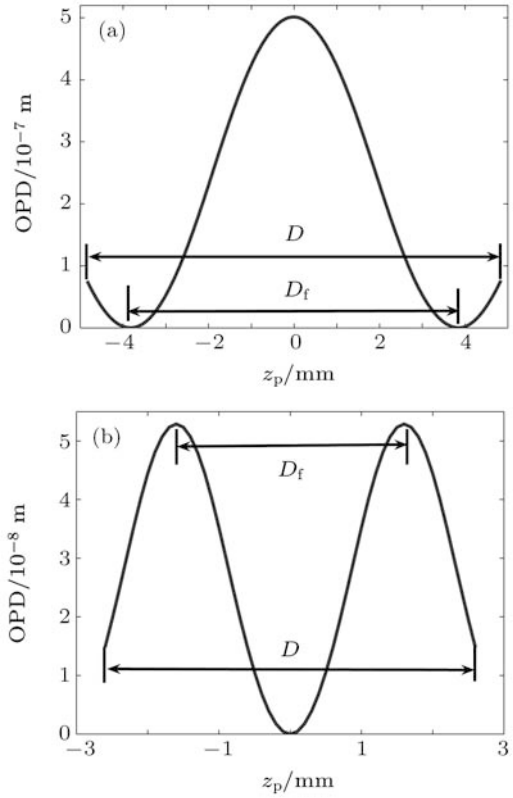


Fig. 3. OPDs versus relative projection position at TIR face for (a) $N = 10$ and (b) $N = 24$.

The OPD data can be obtained by substituting the solved $T(x, y, z)$ into Eqs. (6)–(8). We focus on the comparison of the OPDs experienced by the beam paths going through different positions along the projection length D of the full-aperture beam at the TIR face. Figure 3 describes the OPD versus relative projection position $z_{\rm p}$ at the TIR face for the cases of $N = 10$ and $N = 24$ respectively. The OPD is periodic versus $z_{\rm p}$ with a period of $D_{\rm f}$. It is because that arbitrary two beam paths with the $z_{\rm p}$ difference of $D_{\rm f}$ is symmetric with respect to the $y = 0$ axis, thus they experience the same total value of OPD along the zigzag path owing to the symmetry of the dual-end pumping configuration. The main lobe of the OPD curve, i.e., the central portion with a $z_{\rm p}$ range of $D_{\rm f}$, is close to the parabolic OPD profile of the imaginary ideal lenses. The beam size of light within the main lobe is referred to as the main lobe aperture, and the other portion is called the side lobe aperture.

In Fig. 3, the maximum OPD value occurs at $z_{\rm p} = 0$ for $N = 10$, while the minimum OPD value appears at $z_{\rm p}$=0 for $N = 24$, which means that the thermal lens along the slab thickness direction for the main lobe aperture varies between the convex lens and the concave one surprisingly only with incident angle $\theta = 67.1°$ for $N = 10$ and $\theta = 24.2°$ for $N = 24$. To clarify the reason why the curvature type varies, the temperature distribution in the cross section is replotted in the $x'y'z'$ coordinate system with $z_{\rm p}$ as the variable of the vertical axis, as shown in Fig. 4. It is pointed out in Fig. 4(a) that the ray at $z_{\rm p}$=0 passes through the two hottest regions in the slab located at the interfaces between the gain medium cap and the undoped one. In comparison, the average temperature along the route, through which the ray (dashed line) on the edge of the main lobe aperture travels, is much lower, therefore the thermally induced lensing appears as a convex lens. The formation of the concave lens for the case of $N = 24$ shown in Fig. 4(b) can be well explained in a similar way.

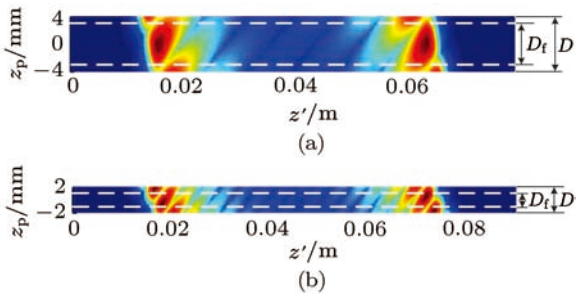


Fig. 4. (colour online) Temperature profiles in y'–z' cross section for (a) $N = 10$ and (b) $N = 24$.

For the slab parameters presented in Section 3, the available N for the full-aperture beam passing through the slab ranges from 8 to 36, which is limited by the incident angles at the slab ends (the corresponding θ ranges from 3.3° to 85.8°). However, if we consider the SiO_2 coatings deposited on the TIR surfaces, which reduces the loss from the evanescent wave, it is required that $\gamma < 90°$–$\theta_{\rm crit} = 90°$–arcsin (1.46/1.82)=36.7°, thus N should be no more than 28.[14] Figure 5 shows the variation of the focal length of the corresponding thermal lens with the total number of bounces N for the main lobe aperture, indicating that the absolute value of the maximal OPD is

reduced while the focal length is enhanced with the raise of N. The case of $N = 28$ corresponds to a focal length of 6.46 m. As the number of bounces increases consecutively, the curvature type of the thermal lens in the slab thickness direction oscillates between the concave lens and the convex one, but not in an alternate manner. It should be noted that although the zigzag propagation with larger N benefits from the weaker thermal lensing as well as the higher fill factor,[13] the ratio of $D_{\rm f}$ to D becomes smaller and smaller, leading to a larger portion of the side lobes and thus bringing more serious deformation in the beam transverse mode.

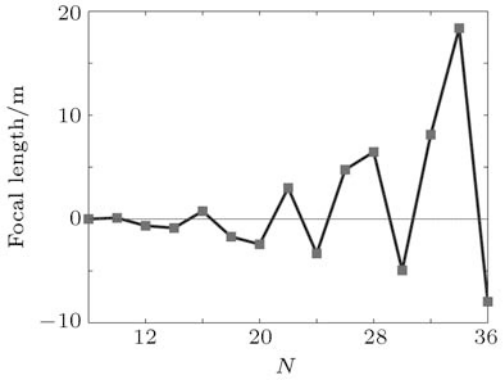


Fig. 5. Dependence of focal length of the thermal lens on N.

4. Conclusion

We investigate the thermal lensing along the direction of heat removal in a zigzag slab laser by numerically computing its temperature distribution, the OPD profile and the focal length of the thermal lens. Particular attention is paid to the dependence of the curvature type of the thermal lens on the number of bounces. The analysis and the discussion provide a good reference for the design of slab parameters and the selection of the number of bounces. Furthermore, multiple zigzag slabs with different curvature types of thermal lenses can be placed in a cavity or lined up as a multi-stage amplifier, which may compensate the thermal lensing and the wavefront deformation, thus improving the beam quality.

References

[1] Shine R J, Aifrey A J and Byer R L 1995 *Proc. SPIE* **2379** 112

[2] Mandl A, Zavriyev A, Klinmek D E and Ewing J J 1997 *IEEE J. Quantum Electron.* **33** 1864

[3] Tei K, Kato M, Niwa Y, Harayama S, Maruyana Y, Matoba T and Arisawa T 1998 *Opt. Lett.* **23** 514

[4] Eggleston J M, Albercht G F, Petr R A and Zumdieck J F 1986 *IEEE J. Quantum Electron.* **22** 2092

[5] Goodno G D, Komine H, McNaught S J, Weiss S B, Redmond S, Long W, Simpson R, Cheung E C, Howland D, Epp P, Weber M, McClellan M, Sollee J and Injeyan H 2006 *Opt. Lett.* **31** 1247

[6] Yasuhara R, Kawashima T, Sekine T, Kurita T, Ikegawa T, Malsumoto O, Miyamoto M, Kan H, Yoshida H, Kawanaka J, Nakatsuka M, Miyanaga N, Izawa Y and Kanabe T 2008 *Opt. Lett.* **33** 1711

[7] Sridharan A K, Saraf S, Sinha S and Byer R L 2006 *Appl. Opt.* **45** 3340

[8] Fu X, Liu Q, Yan X P, Cui J Y and Gong M L 2010 *Laser Phys.* **20** 1707

[9] Fu X, Liu Q, Yan X P, Cui J Y and Gong M L 2011 *Laser Phys.* **21** 48

[10] Shoup M J, Kelly J H and Smith D L 1997 *Appl. Opt.* **36** 5827

[11] Chen B, Chen Y, Simmons J, Chung T Y and Bass M 2006 *Appl. Phys.* B **82** 413

[12] Chung T and Bass M 2007 *Appl. Opt.* **46** 581

[13] Fu X, Liu Q, Yan X P, Cui J Y and Gong M L 2009 *Chin. Opt. Lett.* **7** 6

[14] Koechner W 1970 *Appl. Opt.* **9** 2548

[15] Bermudez J, Pinto-Robledo V, Kiryanov A and Damzen M 2002 *Opt. Commun.* **210** 75

[16] Macdonald M, Graf T, Balmer J and Weber H 2000 *Opt. Commun.* **178** 383

[17] Xiong Z, Li Z, Moore N, Huang W and Lim G 2003 *IEEE J. Quantum Electron.* **39** 979

[18] Goodno G, Palese S, Harkenrider J and Injeyan H 2001 *Opt. Lett.* **26** 1672